

Can piezoelectric accelerometers be used to actively damp the mechanical suspensions in laser interferometric gravitational wave detectors

P. J. Veitch

Department of Physics and Mathematical Physics, University of Adelaide, South Australia 5005, Australia

J. Hough, E. Morrison, and D. I. Robertson

Department of Physics and Astronomy, University of Glasgow, Glasgow G12 8QQ, Scotland

(Received 24 August 1995; accepted for publication 4 December 1995)

An investigation of the use of mass-loaded piezoelectric accelerometers for active damping of high Q , mechanical, vibration isolation suspensions is reported. The transfer function and noise of the accelerometer are modeled, and the predicted noise compared with measurements. A servo which damps the normal modes of a two-stage suspension by sensing the acceleration of, and feeding back to, the intermediate mass is then modeled. The rms and "high frequency" closed loop motions of the isolated mass are calculated. © 1996 American Institute of Physics. [S0034-6748(96)01003-1]

I. INTRODUCTION

Laser interferometric gravitational wave detectors endeavor to detect the passage of a burst of gravitational radiation by sensing the change in the relative separation of a number of almost-freely suspended test masses using laser interferometry.¹ To allow unambiguous detection of the minute changes in separation that are expected,² the test masses must be isolated from many external influences. In particular, the test masses must be highly isolated from seismic vibrations and, further, the parts of the suspension nearest each test mass must not apply significant Nyquist dissipation-fluctuation forces to the suspension. That is, the "last stages" of the test mass suspension must have low mechanical losses. However, the concomitant high Q normal modes can result in large motions of the test masses at the normal mode frequencies. This can lead to difficulties in the servo control of the positions of the test masses since the energy stored in this motion must be extracted by the servo before control can be achieved, and the motion may exceed the dynamic range of the transducer. Further, the high Q 's may affect the stability of the servo.³

The high Q normal modes can be damped by implementing a servo control which uses either an inertial or non-inertial sensor to monitor the motion of the suspended masses, and then applies a correction force to the appropriate part of the suspension system.³ An example of a noninertial sensor is a shadow-position sensor,⁴ as used on prototype interferometers, which consists of a flag that is mounted on the sensed surface and is free to move between a light-emitting diode and photodiode that are mounted on a reference surface. However, this type of sensor has the disadvantage that it is as sensitive to the motion of the reference surface as it is to motion of the sensed surface; which could result in high frequency vibrations being imposed on the suspended test mass unless the reference surface was sufficiently well isolated from environmental and seismic vibrations.³ Further, a noninertial sensor is sensitive only to the relative motion of the sensed and reference surfaces. Thus, if a suspended reference mass was used then the non-inertial sensor would not damp the common mode motion of the test and reference masses.

An inertial sensor such as a mass-loaded piezoelectric accelerometer does not have these problems; but perhaps would appear to have a more serious problem in that it does not have much sensitivity to low frequency displacements. We will show, however, that such a sensor may be used in a normal-mode damping servo without introducing excessive noise.

We will consider the two-stage suspension system shown in Fig. 1. The motion of the intermediate mass is sensed using a mass-loaded piezoelectric accelerometer. The model assumes that the correction force is applied to the intermediate mass using a magnetic actuator similar to those used in prototype interferometers.⁴ To decide whether the piezoelectric accelerometer is suitable, we need to determine the signal produced by the accelerometer and the noise produced by the piezoceramic and preamplifier. These parameters can then be used to calculate the closed-loop noise imposed on the test mass by a realistic servo loop. Clearly we require that the servo electronic noise not limit the sensitivity of the detector at its operating frequencies (>100 Hz), and that the residual low frequency noise imposed on the test mass by the servo noise be less than the residual low frequency noise due to seismic excitation.

This control system is an example of an active vibration isolation system in which only the Q of the mechanical system is controlled. Active isolation systems can also be used to increase the isolation by using feedback to actively reduce the mechanical resonant frequency.⁵ However, such control systems require more complex sensors which have better low frequency sensitivity.

II. PIEZOELECTRIC ACCELEROMETER AND PREAMPLIFIER

Piezoelectric accelerometers can be configured to apply either a compressive or shear stress to the piezoceramic.⁶ However, the best sensitivity and the lowest pyroelectric induced noise is obtained by operating the piezoceramic in shear mode.

The output of the piezoceramic can be preamplified using either a charge-sensitive amplifier, which converts the charge induced on the electrodes of the piezoceramic by the

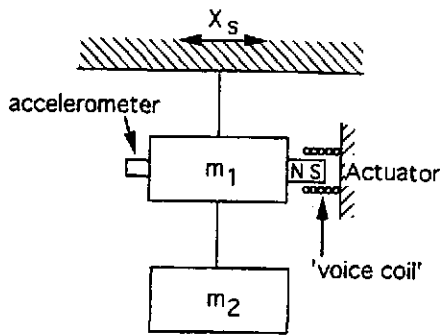


FIG. 1. Schematic of the two-stage suspension considered in this paper. The signal from the accelerometer is amplified and filtered, and then feedback to the "voice coil" which applies a force to the magnet mounted on the intermediate mass.

applied stress to an output voltage, or a noninverting voltage amplifier which amplifies the potential difference induced across the piezoceramic electrodes by the applied stress. We begin this section by predicting that the signal-to-noise ratio obtained when using a charge-sensitive amplifier will be very similar to that obtained using a voltage amplifier, and conclude by demonstrating that the predicted noise for the charge configuration is in good agreement with experiment.

A. Signal at the output of the preamplifier

The induced charge and induced voltage are given by

$$\text{induced charge} = m\omega^2 x_0 d_{15} \quad (1)$$

$$\text{induced voltage} = \frac{m\omega^2 x_0 d_{15}}{C_p} \quad (2)$$

where m is the mass of the inertial load, ω is the angular frequency of the applied stress, x_0 is the amplitude of the motion, d_{15} is the charge density/shear stress at constant electric field, and C_p is the capacitance of the piezoceramic.

To determine the voltage that appears at the output of the preamplifier we need to model the cable that connects the piezoceramic to the preamplifier, and the amplifier. Neglecting the various noise generators for the moment, the accelerometer and preamplifier can be modeled as shown in Fig. 2.

At frequencies well below the internal resonant frequency of the piezoceramic (which is ideally $>$ several kHz), the signal at the output of the charge-sensitive amplifier is given by

$$V_{\text{out}} \approx \frac{-jm\omega^3 x_0 d_{15} R_f'}{(1 + j\omega C_f R_f')} \quad (3)$$

provided that $A_{OL} C_f \gg C_p + C_c$ and $A_{OL} R_{p||d} \gg R_f'$, where A_{OL} is the open-loop gain of the op-amp, $R_{p||d} = R_p R_d / (R_p + R_d)$, $R_f' = (1 + R_1/R_2) R_f$, and R_d is the input impedance of the op-amp. Thus, the output signal produced by the charge-sensitive amplifier configuration is unaffected by the cable capacitance.

Similarly, the signal at the output of the voltage amplifier is given by

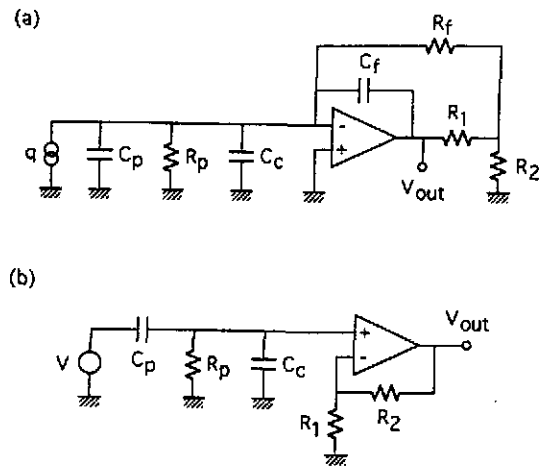


FIG. 2. The models used to determine the transfer function of the piezoceramic accelerometer and (a) a charge-sensitive preamplifier, and (b) a voltage preamplifier. C_p and R_p represent the capacitance and leakage resistance of the piezoceramic. C_c represents the capacitance of the cable that connects the accelerometer to the preamplifier. Note that the feedback resistor R_f is required to limit the dc gain of the charge-sensitive preamplifier. It results in additional phase advance of the signal, however, and this phase advance must be subsequently corrected if the signal is to be used in a servo loop.

$$V_{\text{out}} \approx \frac{jm\omega^3 x_0 d_{15} R_p \left(1 + \frac{R_2}{R_1}\right)}{1 + j\omega(C_p + C_c)R_p} \quad (4)$$

provided that $R_d \gg R_p$. Note that the cable capacitance attenuates the signal from the piezoceramic.

Thus, the charge-sensitive amplifier configuration would appear to be better. However, this conclusion neglects the noise produced by each configuration, and consideration of the signal-to-noise ratio indicates that there is very little difference between the two configurations.

B. Noise at the output of the preamplifier

An expression for the noise at the output of the preamplifier can be determined using the models shown in Fig. 3. It can be shown that the spectral density of voltage noise at the output of the charge-sensitive amplifier is given by

$$S_{n,\text{out}} \approx \left(\frac{R_f'^2}{1 + \omega^2 C_f^2 R_f'^2} \right) \left\{ \left[\frac{1 + \omega^2 (C_p + C_c)^2 R_{f||p}^2}{R_{f||p}^2} \right] S_{v,\text{eff}}^q + 4k_B T \omega C_p \tan \delta + S_{i,\text{eff}}^q \right\} \quad (5)$$

where

$$R_{f||p} = R_f R_p / (R_f + R_p),$$

$$S_{v,\text{eff}}^q = S_v + |Z_{3||}|^2 \left(S_i + \frac{4k_B T}{R_3} \right),$$

$$S_{i,\text{eff}}^q \approx S_i + \frac{4k_B T}{R_f} + \frac{4k_B T}{R_p},$$

$$Z_{3||} = R_3 / (1 + j\omega C_3 R_3),$$

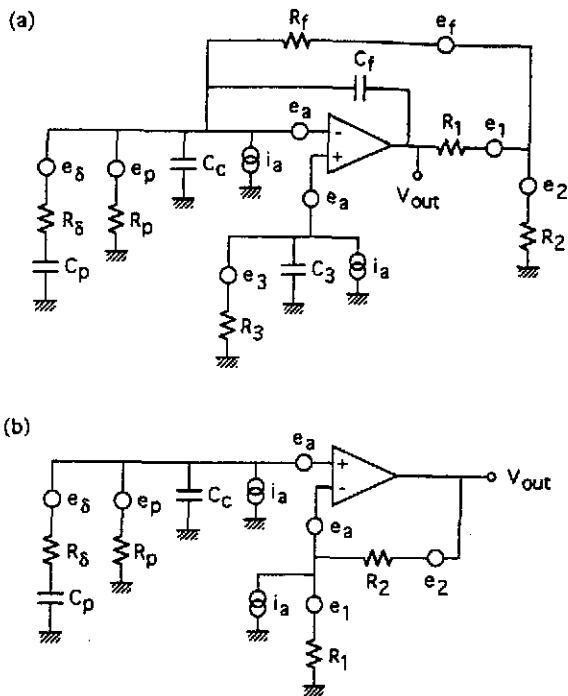


FIG. 3. The models used to determine the noise at the output of the (a) charge-sensitive preamplifier, and (b) voltage preamplifier. e_p , e_f , e_1 , e_2 , and e_3 represent the Johnson noise produced by the associated resistors. e_δ represents the Johnson noise produced by the resistance associated with the loss tangent of the piezoceramic, $R_\delta = \tan \delta \omega C_p$. e_a and i_a represent the equivalent input voltage and current noise of the op-amp; they are related to the more usually specified (single-sided) equivalent input noises e_n and i_n by $e_a^2 = e_n^2/2$ and $i_a^2 = i_n^2$.

S_v and S_i are the spectral density of voltage and current noise of the op-amp, and $\tan \delta$ is the loss tangent of the piezoceramic. The derivation of Eq. (5) assumed that $\tan \delta \ll 1$, R_1 and $R_2 \ll R_f$ and $C_f \ll C_p$.

$$SNR_q^2 = \frac{m^2 \omega^6 x_0^2 d_{15}^2}{\left[\frac{1 + \omega^2 (C_p + C_c)^2 R_f^2}{R_p^2} \right] \left\{ S_{v,eff}^q + 4k_B T \omega C_p \tan \delta + S_{i,eff}^q \right\}}, \quad (7)$$

and the SNR for the voltage configuration, SNR_v , is given by

$$SNR_v^2 = \frac{m^2 \omega^6 x_0^2 d_{15}^2}{\left[\frac{1 + \omega^2 (C_p + C_c)^2 R_p^2}{R_p^2} \right] \left\{ S_{v,eff}^v + 4k_B T \omega C_p \tan \delta + S_{i,eff}^v \right\}}. \quad (8)$$

In practice $S_{v,eff}^q \approx S_{v,eff}^v$, $S_{i,eff}^q \approx S_{i,eff}^v$, and $R_f \gg R_p$, and thus $SNR_q \approx SNR_v$. The remainder of the paper will therefore consider only the charge configuration.

D. Frequency dependence of the output noise

To elucidate the frequency dependence of the noise at the output of the CSA, it is convenient to rewrite Eq. (5) as follows:

Similarly, the spectral density of voltage noise at the output of the voltage amplifier is given by

$$S_{n,out} \approx \left(1 + \frac{R_2}{R_1} \right)^2 \left\{ S_{v,eff}^v + \left[\frac{R_p^2}{1 + \omega^2 (C_p + C_c)^2 R_p^2} \right] \times \{ 4k_B T \omega C_p \tan \delta + S_{i,eff}^v \} \right\}, \quad (6)$$

where

$$S_{v,eff}^v \approx S_v + 4k_B T R_{1||2} + S_i R_{1||2}^2,$$

$$S_{i,eff}^v = S_i + \frac{4k_B T}{R_p},$$

$$R_{1||2} = R_1 R_2 / (R_1 + R_2),$$

assuming $\tan \delta \ll 1$.

C. Signal-to-noise ratio

Using the above equations, the signal-to-noise ratio for the charge configuration, SNR_q , is given by

$$S_{n,out} \approx \left(\frac{R_f^2}{1 + \omega^2 C_f^2 R_f^2} \right) \left\{ \omega^2 (C_p + C_c)^2 S_{v,eff} + 4k_B T \omega C_p \tan \delta + S_{i,eff} \right\}, \quad (9)$$

where

$$S_{v,eff} = S_{v,eff}^q.$$

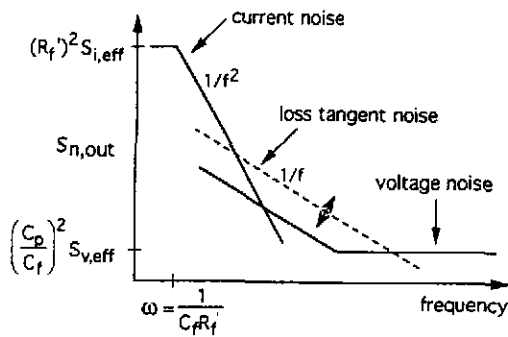


FIG. 4. Contributions to the voltage noise at the output of the charge-sensitive amplifier. We have assumed that the input current noise of the amplifier is white, and that input voltage noise is white at high frequencies but has a flicker component at low frequencies. The noise due to the loss tangent of the piezoceramic will only be evident for sufficiently poor loss tangents.

$$S_{i,eff} = S_{i,eff}^q + \frac{S_{v,eff}^q}{R_{f||p}^2}$$

The frequency dependence of the noise spectral density can be summarized as shown in Fig. 4. At high frequencies the noise is dominated by effective voltage noise ($S_{v,eff}$) which is white at high frequencies and is proportional to approximately $1/f$ at low frequencies. In this frequency range

$$S_{n,out} \approx \left(\frac{C_p + C_c}{C_f} \right)^2 S_{v,eff} \quad (10)$$

The noise contribution due to the loss tangent of the piezoceramic is also proportional to $1/f$ (assuming the loss tangent itself is independent of frequency) and will only be significant relative to the voltage noise contribution if the loss tangent is large. At low frequencies the noise becomes dominated by the effective current noise:

$$S_{n,out} \approx \left(\frac{R_f'^2}{1 + \omega^2 C_f^2 R_f'^2} \right) S_{i,eff} \quad (11)$$

E. Comparison of predicted output noise with measurements

To show that the model accurately predicts the output noise, it is important that the values of the components in the model are determined independently of any noise measurement. Fortunately, it is possible to independently determine most of the component values.

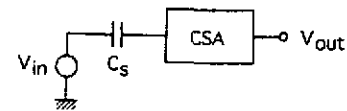


FIG. 5. Circuit used to determine component values in the charge-sensitive amplifier.

The actual values of C_f and R_f' can be determined using the circuit shown in Fig. 5, which has a gain given by

$$\text{gain} = \omega C_s \left\{ \frac{R_f'^2}{1 + \omega^2 C_f^2 R_f'^2} \right\}^{1/2} \quad (12)$$

The gain is largest at high frequencies where it has the value C_s/C_f , and at $\omega = \omega_{3\text{ dB}} = 1/C_f R_f'$ the gain is 3 dB less than the maximum. Thus, measurement of the maximum gain and $\omega_{3\text{ dB}}$ will allow the actual values of C_f and R_f' to be calculated. Our CSA has $C_f = 3.25$ pF and $R_f' = 1.68 \times 10^{10}$ Ω .

$S_{i,eff}$ can be estimated by placing a low capacitance, low loss tangent, high leakage resistance (polystyrene) capacitor on the input of the CSA and measuring the noise on the output at a sufficiently low frequency that the loss tangent and effective voltage noise contributions are negligible (0.1 Hz, for example). Equation (11) can then be used to calculate $S_{i,eff}$. Our CSA has $S_{i,eff} = 1.27 \times 10^{-30}$ A²/Hz, which is close to that calculated using the specified⁷ input current noise ($S_i^{1/2} = 0.3$ fA/ $\sqrt{\text{Hz}}$) and $R_p = 1 \times 10^{11}$ Ω . The contribution to $S_{i,eff}$ due to $S_{v,eff}$ is negligible. Since the effective current noise is dominated by the Nyquist noise from R_f and the leakage resistance of the piezoceramic is expected to be $> 10^{11}$ Ω , the above value of $S_{i,eff}$ should be a good estimate of the effective current noise of the accelerometer and CSA. Note that $S_{i,eff}$ will be independent of frequency as S_i is frequency independent.⁷

The most accurate method of determining $S_{v,eff}(\omega)$ is to measure the output noise when the input is loaded by a selection of low loss-tangent (polystyrene) capacitors which maximize the output noise due to $S_{v,eff}$ but do not produce an amplifier gain that exceeds the open-loop gain of the op-amp. Then, since $S_{i,eff}$ has already been determined and $\tan \delta \approx 5 \times 10^{-4}$ for low-loss polystyrene capacitors, Eq. (9) can be used to calculate $S_{v,eff}(\omega)$. For the CSA shown in Fig. 2, we used a 9950 pF capacitor to determine the 0.1–50 Hz noise, a 1158 pF capacitor to determine the 100–500 Hz noise, and a 241 pF capacitor to determine the 1–5 kHz noise. We obtained $S_{v,eff}^{1/2} \approx 8.0$ nV/ $\sqrt{\text{Hz}}$ at high frequencies, and the low-frequency corner was at ~ 100 Hz.

To check the model's predictions a piezoceramic device that had minimal sensitivity to mechanical vibrations was constructed. It consisted of two shear-plate Pz26 piezoceramics⁸ that were bonded to an end-face of a brass cylinder, with their polarization axes pointed in opposite directions, and electrically connected in parallel. The ceramics had been annealed after polarization so as to minimize aging. Thin wires were used to connect the device to the CSA. The parameters of the compound piezoceramic were $C_p = 376$ pF and $\tan \delta = 3 \times 10^{-3}$. The measured output noise and the predicted noise are shown in Fig. 6. Note that the agreement is very good, and so the accelerometer-CSA model can be

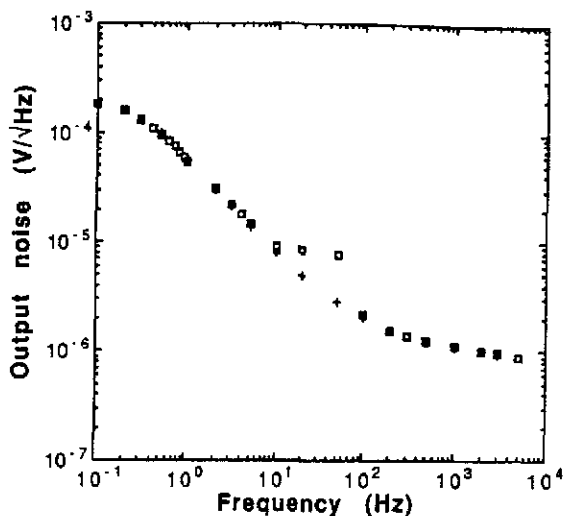


FIG. 6. The measured (box symbols) and predicted (plus symbols) noise at the output of the charge-sensitive amplifier.

used with confidence to predict the residual noise in the servo loop. The disagreement between the measurements and predictions at 20 and 50 Hz is due to environmental mechanical noise.

Figure 7 illustrates how the loss tangent of the piezoceramic affects the output noise: for $C_p=376$ pF, $\tan \delta \approx 1 \times 10^{-3}$ is required to remove the effect of loss tangent noise. A Pz26 ($d_{15} \approx 400$ pC/N)⁸ accelerometer with an inertial mass of 1 kg and $C_p=376$ pF would have an open-loop displacement sensitivity of about 4×10^{-14} m/ $\sqrt{\text{Hz}}$ at 100 Hz. In contrast, the higher loss tangent noise in a Pz29 ($d_{15} \approx 700$ pC/N, $\tan \delta \approx 2 \times 10^{-2}$) accelerometer that had the same geometry (and therefore different C_p) would result in a sensitivity of about 7×10^{-14} m/ $\sqrt{\text{Hz}}$ at 100 Hz.

III. ACTIVE DAMPING OF A TWO-STAGE PENDULUM SUSPENSION

The loop diagram of the active damping servo model is shown in Fig. 8 and analyzed in the Appendix. The support

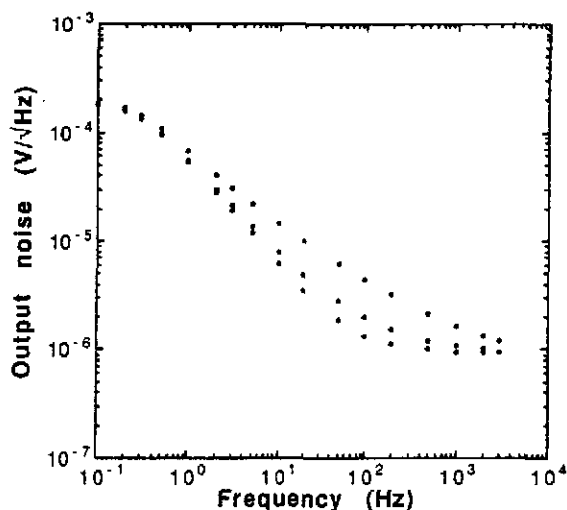


FIG. 7. An illustration of how the output noise of the charge-sensitive amplifier would increase as the loss tangent of the piezoceramic was increased from 5×10^{-4} to 3×10^{-3} to 2×10^{-2} .

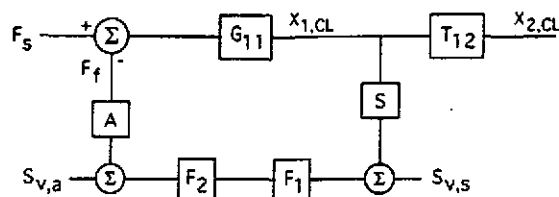


FIG. 8. Servo loop diagram used to model the active damping of the normal modes in a two-stage pendulum suspension. F_s represents the force applied to the intermediate mass due to the motion of the pendulum suspension point. G_{11} represents the open loop response of the intermediate mass to an applied force. The transfer function of the piezoelectric accelerometer and preamplifier is represented by S . The signal from the preamplifier is amplified using a filter with transfer function F_1 to ensure stability of the servo loop, and a filter with transfer function F_2 to remove excess noise at high frequencies. The signal from the second filter is converted to a current and fed to the actuator which has a transfer function A . T_{12} relates the closed-loop motion of the test mass to that of the intermediate mass. The electronic noise added to the loop is represented by $S_{v,s}$, the output voltage noise of the preamplifier, and $S_{v,a}$, the input voltage noise of the actuator. The input voltage noise of the filters is negligible.

point of the suspension experiences a displacement $X_s(s)$ due to seismic (and other environmental) vibrations which, in turn, exerts a force $F_s(s)$ on the intermediate mass and produces motion of the intermediate and test masses. The motion of the intermediate mass is detected using the piezoceramic accelerometer and charge-sensitive preamplifier (S) discussed above. The signal from the preamplifier is filtered (F_1) to ensure loop stability, and the excess high frequency noise is removed using a low-pass amplifier (F_2). The signal is then converted to a current and fed to a noncontacting magnetic actuator (A) which applies a correction force $F_f(s)$ to the intermediate mass. The accelerometer should use a large inertial mass to maximize its sensitivity and minimize the effect of noise, particularly low frequency noise added by the preamplifier.

The closed loop response of the intermediate mass to $F_s(s)$ can be determined using

$$X_{1CL}(s) = \frac{G_{11}(s)F_s(s)}{1 + G_{11}(s)H(s)}, \quad (13)$$

where $H(s) = S(s)F_1(s)F_2(s)A(s)$. The closed loop motion of the test mass, $X_{2CL}(s)$, can be deduced from the motion of the intermediate mass using $X_{2CL}(s) = T_{12}(s)X_{1CL}(s)$, as outlined in the Appendix.

A. Servo loop stability

We can ensure that the servo loop is stable and obtain acceptable transient response by requiring that $2\pi/3 > \arg(G_{11}H) > -2\pi/3$ while $|G_{11}H| > 0$ dB.

The low frequency behavior of $G_{11}H$ is dominated by G_{11} and S in the absence of F_1 . $|G_{11}|$ is independent of s below the coupled mechanical resonant frequency of the intermediate mass and then "rolls-off" as s^{-2} . From Eq. (3),

$$S(s) \approx \frac{ms^3 d_{15} R_f'}{(1 + sC_f R_f')} \quad (14)$$

and thus $|S|$ increases as s^3 at very low frequencies (below the corner frequency of the CSA) and then increases as s^2 .

Therefore, $|G_{11}H|$ would increase as s^3 at very low frequencies, and then increase as s^2 until the mechanical resonant frequency, after which it would become independent of s . Thus, at very low frequencies, the loop gain ($G_{11}H$) would have a $3\pi/2$ phase lead, which must be reduced to less than π before $|G_{11}H|$ becomes larger than 0 dB.

To ensure stability, F_1 must provide some phase lag at low frequencies. That is, it must be a low-pass filter:

$$F_1(s) = \frac{-G_1}{[1 + (s/\omega_{c1})]} \quad (15)$$

with a corner frequency, ω_{c1} , below the mechanical resonant frequency. The optimum position of the low-pass corner will

intermediate mass	$m_1 = 10$ kg	$\omega_1/2\pi = 0.7$ Hz	$Q_1 = 10^6$	
test mass	$m_2 = 10$ kg	$\omega_2/2\pi = 0.7$ Hz	$Q_2 = 10^6$	
accelerometer	$m = 1$ kg	$d_{15} = 400$ pC/N	$C_p = 500$ pF	$R_p = 1 \times 10^{11} \Omega$
	$\tan \delta = 3 \times 10^{-3}$			
CSA	$C_f = 3.25$ pF	$R_f = 1.68 \times 10^{10} \Omega$	$R_1 = 29$ k Ω	$R_2 = 1$ k Ω
filter F_1	$\omega_{c1}/2\pi = 0.065$ Hz			

In addition, we have assumed that the noise reduction filter, F_2 , is a two-pole Chebyshev (2 dB) low-pass filter with a corner frequency $\omega_{c2}/2\pi = 5$ Hz and a transfer function⁹

$$F_2(s) = \frac{K(f_n \omega_{c2})^2}{s^2 + s f_n \omega_{c2} (3 - K) + (f_n \omega_{c2})^2}, \quad (16)$$

where $K = 2.114$ and $f_n = 0.907$.¹⁰

The drive-stage amplifier is assumed to have the circuit shown in Fig. 10, and thus the actuator has a transfer function

$$A(s) = \frac{(1/R_g) F_{dc}}{[1 + s(L_c/R_{||})]}, \quad (17)$$

where $L_c = 20$ mH, $R_{||} = 1$ k Ω , and F_{dc} is the dc force per ampere that would be applied by the actuator. The value of R_g is determined by the required (dc) dynamic range of the actuator. For example, if the maximum output voltage of the op-amps was 10 V and a dynamic range of d_{range} was required then

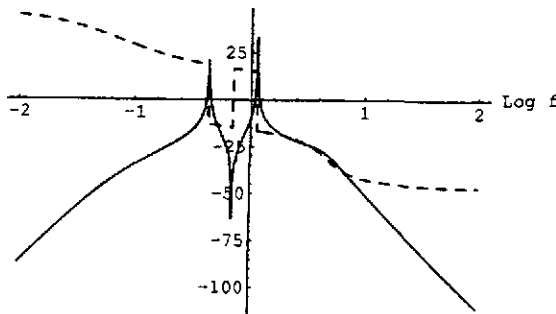


FIG. 9. Bode plots for the assumed servo loop. The solid line is $20 \log[G_{11}H]$ and the dashed line is $10 \arg[G_{11}H]$. The parameters assumed in the calculation are listed in the text.

be determined by the position of the CSA corner frequency relative to the mechanical resonant frequency, and the maximum loop gain required. The net effect should be to yield a phase lead $\approx 2\pi/3$ at the low frequency 0 dB point. An additional effect of F_1 being a low pass filter is that the roll-off of the loop gain above the mechanical resonant frequency will become s^{-1} , and thus ensure that the phase at the upper 0 dB point is also suitable. The servo loop will therefore be stable provided that any phase lags resulting from $F_2(s)$ and $A(s)$ do not significantly degrade the phase margin at the upper 0 dB point.

The Bode plots of the loop gain are shown in Fig. 9. We have assumed the following parameters:

$$R_g = \left(\frac{10V}{d_{range}} \right) \frac{F_{dc}}{G_{11}(s=0)} = \left(\frac{10V}{d_{range}} \right) \frac{F_{dc}}{M \omega_1^2}. \quad (18)$$

Thus, in this particular example, a dynamic range of 0.4 mm would require $R_g = 58 \Omega$ assuming that $F_{dc} = 0.9$ N/A (this corresponds to three prototype magnetic actuators⁴ acting in parallel).

The only remaining free parameter in the servo loop outlined above is G_1 , which can be varied to adjust the damping of the normal modes. However, varying G_1 will also change the servo phase margins which could degrade the servo performance at other frequencies. It can be shown that a normal mode will be critically damped if

$$SF_1 F_2 A|_{s=j\omega_n} = j2m_n \omega_n^2, \quad (19)$$

where m_n and ω_n are the mass and frequency of the normal mode. Thus, in this case, the normal modes will be approximately critically damped if

$$G_1 \approx G_{1c} = -2 \left(\frac{m_1}{m} \right) \left(\frac{\omega_1}{\omega_{c1}} \right) \frac{C_f R_g}{d_{15} K F_{dc}}. \quad (20)$$

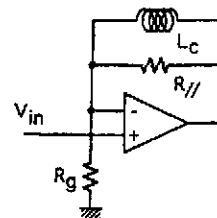


FIG. 10. Circuit diagram of the assumed drive-stage amplifier. L_c is the inductance of the "voice coil" that produces the drive magnetic field. $R_{||}$ prevents saturation of the op-amps at high frequencies.